1. DoE Grant Number DE-AI02-13ER41961 with the Naval Research Laboratory.
2. Project Title: Multipactor Physics, Acceleration, and Breakdown in Dielectric-Loaded Accelerating Structures, Richard P. Fischer, PI, rich.fischer@nrl.navy.mil, 202-404-4355.
3. Date of Report: 30 June 2016, covering the period 1 April 2013 through 31 March 2016.
4. The objective of this 3-year program is to study the physics issues associated with rf acceleration in dielectric-loaded accelerating (DLA) structures, with a focus on the key issue of multipactor loading, which has been found to cause very significant rf power loss in DLA structures whenever the rf pulsewidth exceeds the multipactor risetime (~10 ns). The experiments are carried out in the X-band magnicon laboratory at the Naval Research Laboratory (NRL) in collaboration with Argonne National Laboratory (ANL) and Euclid Techlabs LLC, who develop the test structures with support from the DoE SBIR program. There are two main elements in the research program: (1) high-power tests of DLA structures using the magnicon output (20 MW @11.4 GHz), and (2) tests of electron acceleration in DLA structures using relativistic electrons from a compact X-band accelerator. The work during this period has focused on a study of the use of an axial magnetic field to suppress multipactor in DLA structures, with several new high power tests carried out at NRL, and on preparation of the accelerator for the electron acceleration experiments.

A. DLA experiments at high gradient

This report begins with a discussion of element (1), the study of DLA structures at high gradient without the presence of an electron beam. A new regime of resonant single-surface multipactor in DLA structures was described in our first publication, J.G. Power *et al*., *Phys. Rev. Lett*. **92**, 164801 (2004). A series of subsequent publications from our research collaboration studied the multipactor scaling laws and tested various approaches to suppressing multipactor growth and reducing the multipactor saturation level. These studies tested the effect of different dielectrics and different geometries, in both traveling-wave (TW) and standing-wave (SW) configurations, and also studied the reduction of multipactor by applying low secondary electron emission (SEE) coatings on the dielectric surfaces. Low SEE coatings caused some reduction of the multipactor loading [see C. Jing *et al*., *IEEE Trans. Plasma Sci*. **38**, 1354 (2010)], but were only a partial solution. The focus of the most recent experiments has been the suppression of DLA multipactor with an axial magnetic field, as proposed in two recent theoretical papers [C. Chang *et al., J. Appl. Phys.* **110**, 063304 (2011); O. Sinitsyn *et al*., AIP Proc. **1507**, 505 (2012)]. Chang *et al.* used an analytic model and PIC simulations incorporating that model to show that an axial magnetic field can reduce the period of secondary electrons trajectories on the dielectric surface, and thus spoil a resonance condition associated with multipactor growth in DLA structures. [This is the resonance condition derived by J.G. Power *et al*.] The optimum multipactor suppression is predicted to occur when the ratio of the gyrofrequency to the rf frequency is in the range of ~0.5–2, or ~2–8 kG for an X-band structure, with multipactor predicted to be enhanced below this range and to return at magnetic fields above this range. Sinitsyn *et al.* used a more general PIC model that made no specific assumption about the resonant nature of the multipactor physics and found almost complete suppression of multipactor in a quartz structure at magnetic fields above 4 kG for 5 MV/m gradients, with no return at higher magnetic fields.

The first experimental test of multipactor suppression with an axial magnetic field was carried out prior to the start of this three-year program. The TW DLA operated in the $TM_{01}$ mode, and consisted of an externally metalized alumina tube enclosed in a copper housing for a vacuum seal that was connected to input and output rf couplers via tapered dielectric transitions. Fig. 1 (left) shows the geometry of the structure, the normalized amplitudes of $E_r$ and $E_z$ along the structure, and a profile of the axial magnetic field $B_z$ of the magnet enclosing the structure. The structure was designed to produce an accelerating gradient of 12.5 MV/m at 10 MW input power. The onset of multipactor generally causes a decrease in the rf transmission through a structure accompanied by the emission of light from its inner surface, but may also affect the rf matching and thus change the reflection coefficient. Fig. 1 (center) shows typical rf reflection signals measured by a diode detector with and without an external magnetic field. The input rf pulse was approximately Gaussian, with a peak gradient of 4 MV/m. With $B_z$=0, the reflected signal

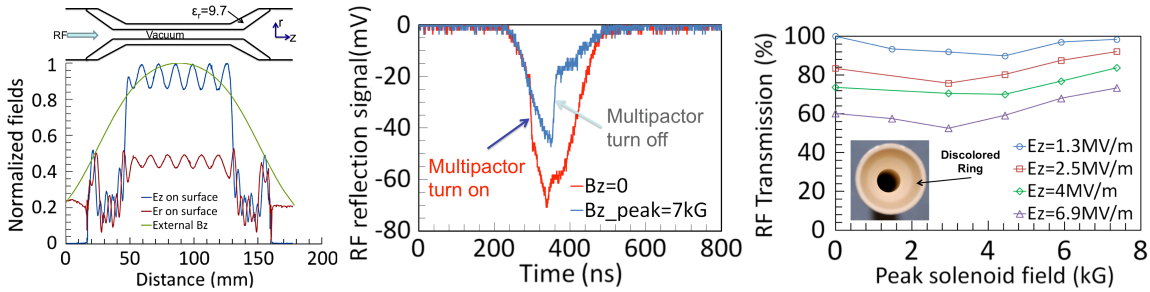


***Fig. 1**. (left) Diagram of the geometry of the alumina structure used in the first experiment, and normalized rf electric fields and magnetic field profile; (center) Comparison of the reflected rf signals at $E_z$=4 MV/m for $B_z$=0 kG and $B_z$=7 kG fields at the center of the structure; (right) Measured rf transmission (in percent) as a function of magnetic field for various values of $E_z$. Inset shows discoloration on the disassembled input end of the structure, indicating intense multipactor loading in the tapered region of the dielectric tube.*

increases sharply as the field rises to ~1 MV/m, indicating the onset of multipactor. This abrupt rise does not occur for $B_z$=7 kG, and there is instead a sharp falloff in the reflected rf signal later in the pulse (at a higher level of rf field), suggesting that multipactor suppression had kicked in. At the same time, the multipactor light emission observed by a video camera focused on the center of the structure was found to disappear and rf transmission improved, also suggesting some level of multipactor suppression. Fig. 1 (right) plots the rf transmission of the DLA structure as a function of $B_z$ at several different accelerating gradients. As predicted by Chang, a weak magnetic field appears to increase the rf loading, while a stronger field (in the optimum range) reduced it. These data also show that a higher accelerating gradient was favorable for multipactor suppression, as predicted by Chang, which is a favorable scaling for high-gradient accelerator applications. However, the rf transmission did not return to the level measured before the onset of multipactor. For $B_z$=0, 40% of the rf power was absorbed when the accelerating gradient was increased from ~1 MV/m to ~7 MV/m, but the transmission at the higher gradient was only improved by ~15% at $B_z$=7 kG. The limited improvement that was observed was attributed to axially non-uniform suppression of the multipactor due to the variation of the electric and magnetic field along the length of the structure. Specifically, it appeared that multipactor was suppressed in the center section of the DLA structure at high magnetic fields (the multipactor light emission from that region vanished), but that it may have been enhanced at lower magnetic field in the tapered regions of the structure. Fig. 1 (right) inset shows the presence of a discolored ring at the input end of the dielectric taper, indicating that intensified electron bombardment occurred in this region, thus supporting this hypothesis.

The results of the first experimental test appeared to demonstrate the beneficial effect of an axial magnetic field to reduce the level of multipactor in a DLA structure, but the presence of nonuniform magnetic fields and tapered rf accelerating fields created uncertainties in the interpretation of the measurements. Therefore, preparation began on new DLA structures that would provide more clear-cut results. The next structure to be tested was an untapered TW structure with uniform accelerating gradient, which was placed in the uniform-field region of a long solenoidal magnet. The new structure used matching irises at either end of the dielectric-lined accelerating region (see Fig. 2 center), thus eliminating the nonuniform rf accelerating fields in the tapered matching regions. However, the new matching irises had a narrower passband than the previous tapered transitions, and this introduced a new problem. When the structure was assembled, it was discovered that the center of its passband had shifted somewhat from the desired operating frequency, causing a mismatch at the ends of the structure that resulted in a substantial reflection coefficient. The magnicon can operate without difficulty into a large mismatch. However, the large reflected signal complicated the interpretation of the experimental results, as discussed below.

To prepare for the experiment, a massive 300 V, 140 A (42 KW) power supply and a 1 ton solenoidal magnet capable of producing a 1.1 T magnetic field were shipped from ANL to NRL in the spring of 2014. The power supply was connected to a new 480V, 50A electrical circuit in the magnicon lab, and new water lines were installed to cool the magnet and the power supply. However, the power supply did

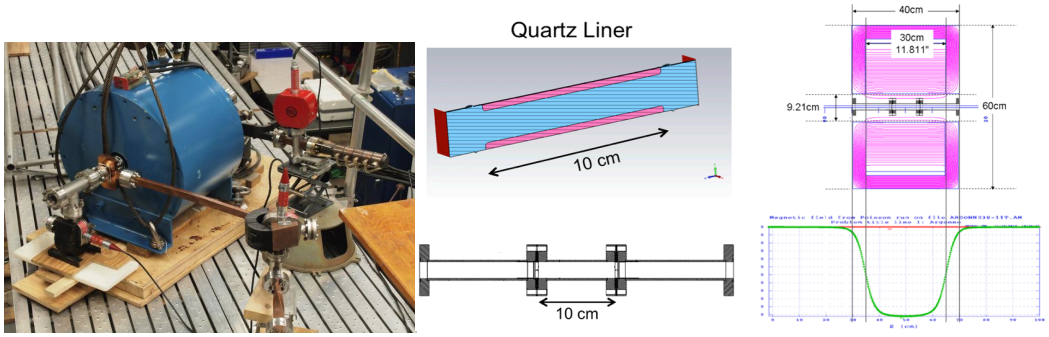


***Fig 2**. Setup for the second test of multipactor suppression with an axial magnetic field. (left) photograph of the setup, (center) geometry of the DLA structure with quartz liner, (right) magnetic field configuration.*

not arrive in working order, and several weeks of intense effort were required to diagnose and repair it. Next, the new magnet was lifted into positioned on the elevated platform (adjacent to the magnicon output) and connected to the power supply with high-current cables. In April 2014, the new TW DLA structure was installed in the bore of the magnet and placed under vacuum. Fig. 2 (left) shows the structure in the bore of the magnet, with the drive waveguide and components seen in the foreground entering the magnet, and the output load emerging from the far end of the magnet at the upper right. Fig. 2 (right) shows a cross section of the magnet and the DLA structure along with the magnetic field profile. The structure fit easily within the uniform field region of the magnet.

The new TW structure was tested at high power using the magnicon output beginning in May 2014. Fig. 3 shows a set of oscilloscope traces taken with no axial magnetic field (left) and with $B_z$=11 kG (right) at 11.9 MW of drive power. These traces show that the most dramatic change caused by the application of the strong axial magnetic field is the reduction in $V_{PD}$, the signal from a photomultiplier monitoring light emission from the structure. The photomultiplier (PMT) is linear in light intensity, and the traces show that the intensity of emitted light from the center of the structure decreased by 65% due to the application of the magnetic field, even though the onset time was unchanged. Our previous experiments on other structures have showed a linear correlation between emitted light intensity and missing microwave power, so the reduced PMT signal suggests a substantial reduction in the multipactor loading. However, in this case the change in the microwave signals is much less dramatic. For identical forward powers, the "missing power" not accounted for by transmission or reflection, and thus attributed to multipactor loading inside the structure, decreased by only 37% (3.45 MW to 2.19 MW). Moreover, most of the reduction in missing power is accounted for by a large increase in reflected power (3.88 MW – 2.83 MW = 1.05 MW), rather than the much smaller increase in transmitted power (~0.24 MW). Apparently, the primary effect of the axial magnetic field was a significant change in the microwave matching of the structure. These somewhat inconclusive results illustrate the difficulty that the mismatched structure caused in interpreting the experimental results.

Fig. 4 shows a summary of the multipactor data from this experiment. Raising the magnetic field progressively reduces the multipactor light emission at gradients of 2.3 MV/m and 5 MV/m, while also reducing the missing power. However, at a magnetic field of 1 kG, both light emission and missing power are slightly enhanced for the 5 MV/m data, in apparent agreement with Chang's model where low magnetic fields can enhance the multipactor loading. Fig. 4c shows the overall dependence of multipactor power loss on accelerating gradient at $B_z$=10 kG. The results from this experiment appear to be in partial agreement with the two theoretical papers that have studied this problem, but they both predict strong suppression of multipactor loading with application of the axial magnetic field, while only partial suppression is observed experimentally. In addition, the progressive suppression of

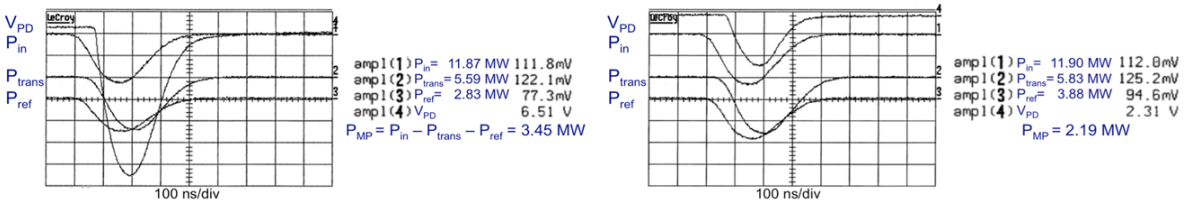


***Fig. 3***. *Oscilloscope traces from second test of multipactor suppression, showing the incident, transmitted and reflected microwave pulses as well the signal from a photomultiplier monitoring light emission from the DLA structure. (left) $B_z$=0 and (right) $B_z$=11 kG.*

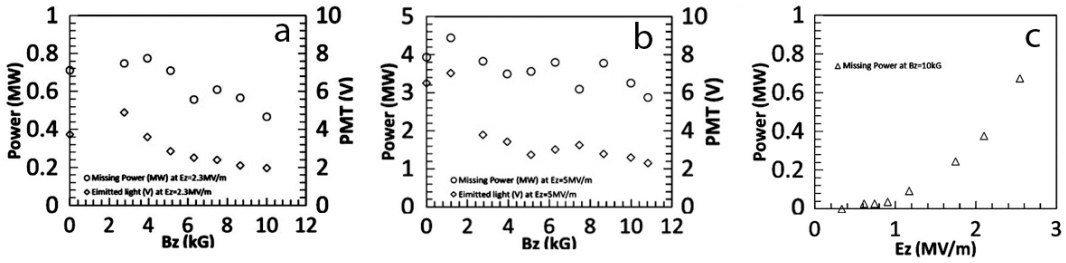


***Fig. 4***. *Experimental data from second test of multipactor suppression with an axial magnetic field: (a) Missing power and multipactor light emission at 2.3 MV/m; (b) Missing power and multipactor light emission at 5 MV/m; (c) Missing power as a function of accelerating gradient at $B_z$=10 kG.*

multipactor at magnetic fields above 8 kG agrees better with Sinitsyn's PIC simulations than with Chang's resonant trajectory model, suggesting that the resonant electron model is incomplete. These matters clearly require better experimental data as well as further theoretical analysis.

A short, well-matched SW structure was tested in December 2014. It had previously been tested at NRL with no magnetic field. The structure lacks an interior rf field probe to directly monitor the cavity fields, so the buildup of rf fields and multipactor loading have to be inferred from the incident and reflected waveforms [see C. Jing *et al*., Proc. 2012 IPAC, pp. 1927–1929 for the procedure employed]. The SW structure was installed in the bore of the large solenoidal magnet and put under vacuum in the magnicon laboratory at NRL on 3 December 2014, and tested at high power during the week of 15 December. Fig. 5 shows a set of waveforms from this experimental run at constant drive power and progressively increasing magnetic field. With $B_z$=0 (left), the reflected waveform increases suddenly at the center of the trace, indicating the onset of multipactor, and then traces a typical cavity response curve for the reflection of a poorly matched cavity. The bump in the tail results when the rf drive power vanishes and stored energy is discharged from the cavity. At 1.2 kG, the reflection also increases at the center of the trace, as multipactor turns on, but then becomes very irregular, suggesting worsening multipactor. At 2.4 kG, multipactor still turns on, but the maximum mismatch is reduced, indicating a lower level of multipactor loading. Then at 3.6 kG, there is little evidence of multipactor onset, and the response curve indicates a well-matched cavity. Also, further increasing the magnetic field in steps up to 9.8 kG made only small additional changes in the reflection waveform. These data show good evidence of the predicted multipactor suppression at high magnetic field, as well as showing poorer performance at the lowest magnetic field (predicted by Chang).

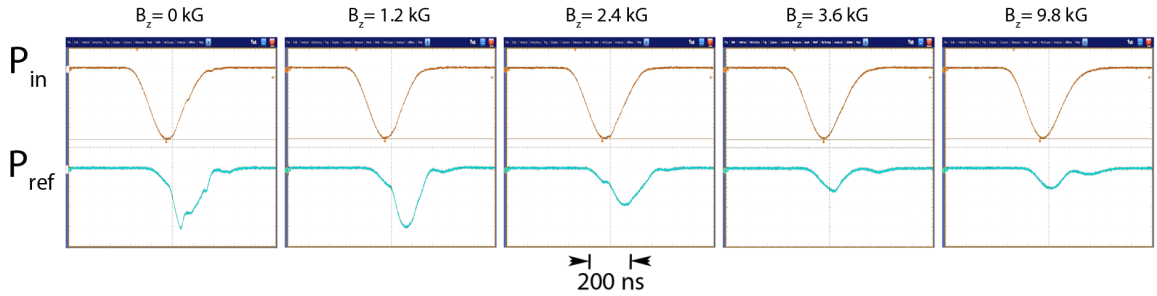


***Fig 5***. *Experimental traces from the SW structure test. (Note that $P_{ref}$ is delayed by ~80 ns.)*

In the Fall of 2015, a new experiment was performed under improved conditions with a uniform axial magnetic field extending along the length of an X-band standing-wave DLA structure. Multipactor loading is continuously reduced starting from 3.5 kG applied magnetic field and is completely suppressed at ~8 kG. Dependence of multipactor suppression on the rf gradient inside the DLA structure is also measured.

This experiment used an improved set up: 1) a large solenoidal magnet capable of producing 1.1 Tesla axial magnetic field over its central 10 cm; 2) a shorter standing wave DLA which consists of a 2.6 cm long dielectric tube to ensure the uniformity of $B_z$ over the entire length of the structure; 3) a built-in rf probe to monitor the accelerating gradient inside the cavity during the experiment. The rf power source used to drive the DLA structure is the same as in the earlier experiment, the 11.4 GHz, 20 MW magnicon at the Naval Research Laboratory. During the experiment, the cavity was conditioned up to 20 MV/m (the value at which arcing occurred at the spot where ceramic, metal, and high electric field are present) on axis with a pulse length of 200 ns FWHM. The behavior of the structure was studied as a function of axial magnetic field at four different rf power levels, and the gradient inside the dielectric cavity was recorded for each. The results are summarized in Fig. 6. There are four distinct multipactor regions that depend upon the strength of the axial magnetic field: 1) Multipactor Bifurcation Regime --- when the externally applied $B_z$ increases from zero to ~1 kG, the accelerating field inside the DLA cavity decreases at low rf drive power but increases at higher levels of rf drive; 2) Multipactor Enhancement Regime --- when $B_z$ is increased up to ~2.4 kG, the multipactor loading becomes stronger and reduces the cavity gradient; 3) Multipactor Mitigation Regime --- the multipactor loading is reduced and gradient increases accordingly when $B_z$ is in the range of ~2.4 kG to ~8 kG; 4) Multipactor Blocking Regime --- $B_z$ > ~8 kG where the multipactor is totally suppressed. It is worthwhile to point out that multipactor can be suppressed once the external magnetic field exceeds a certain value, but its dependence on gradient appears to be weak.

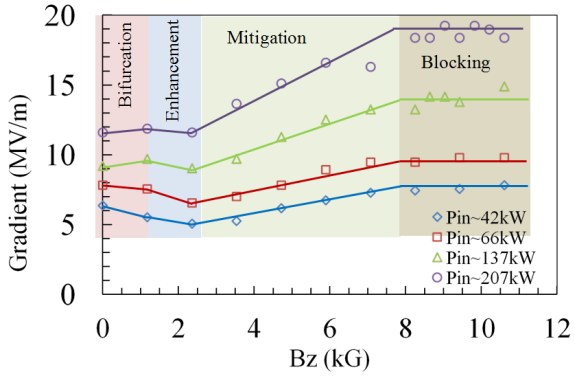


***Fig. 6***. *The dependence of the accelerating gradient on the external axial magnetic field strength for four rf input power levels.*

Fig. 7 shows typical scope traces from the rf probe in regimes 1, 2, and 4. Without the external magnetic field, the signature of multipactor initiation is a sudden gradient dip in the range of 6-7 MV/m, which is close to the previous experimental results after normalizing to the structure length (the gradient is loaded down by the total charge of the secondary electrons in the volume). This initiation threshold drops to 4-5 MV/m when a low-strength solenoid field is applied (less than 2.5 kG in this experiment). However, the accelerating gradient may still increase if the rf power is increased further. In the multipactor-blocking regime, the cavity gradient builds up as in a normal cavity.

Excellent agreement has been obtained between the modeled and measured accelerating gradient signals inside the standing-wave DLA structure. This represents a quantitatively better understanding of multipactor. More importantly, this is the first demonstration of multipactor being fully suppressed in a rf-driven DLA structure. This eliminates one of the most important hurdles towards practical dielectric-based rf linear accelerators and may lead to wide use of dielectric materials in high-field vacuum electronics.

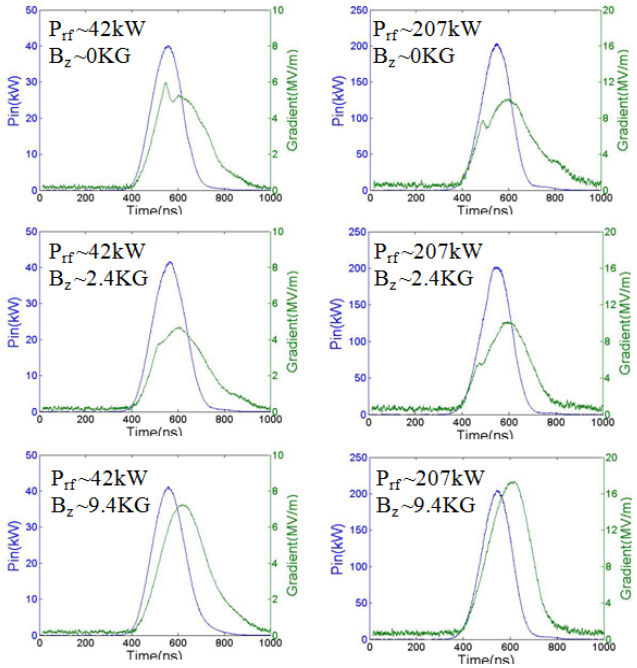


***Fig** 7. Typical scope traces of the different multipactor regions described in Fig. 6.*

B. X-band accelerator experiments

Element (2) of our program is the study of electron acceleration in DLA structures. An X-band electron injector was developed in China and acquired by ANL for this program and installed in a bunker in the Magnicon Laboratory (see Fig. 8). The injector, a 23½-cell disk-and-washer structure with a $LaB_6$ cathode, requires ~5 MW of rf drive to produce a ~5 MeV, 10 mA beam. The accelerator was originally conditioned at NRL with up to 6 MW at 11.4 GHz with no cathode heating. As the cathode was heated, high-energy electrons were produced in the accelerator, where energies up to 4 MeV were measured using the electron spectrometer. Approximately 15 MW of magnicon power is reserved to drive the accelerating structure. The magnicon output (see Fig. 8 (right)) includes a power splitter that can drive two separate waveguides with an adjustable split ratio, so that one output can be used to power the accelerator at constant power while the second output provides an adjustable power to carry out DLA acceleration tests.

Following the initial injector operation, there had been difficulties with cathode arcing followed by a vacuum leak in the cathode stalk that required the cathode to be replaced. In 2013, an electron spectrometer was installed and calibrated at the end of the beam line to enable electron energy measurements. A Be window was installed at the end of the spectrometer output arm, and a PMT and scintillator set in place to permit time-resolved quantitative measurements of the electron energy distribution. Also, a new vacuum waveguide line was built to connect the second magnicon output into the bunker to connect to the DLA test structures. The test structures will be mounted between a pair of bellows at the end of the injector to vary the input phase of the electrons with respect to the rf drive.

Prior to installing the test structure in the beam line, an intense effort was made to propagate the electron beam down to the spectrometer through a small on-axis aperture. Two steering magnets and three focusing quadrupoles were used to align and focus the beam, with YAG:Ce fluorescent screens at both ends of the beam line to monitor the beam position. However, poor emission from the replacement cathode, which appeared to be poisoned, as well as intermittent arcing resulted in unstable operation that made it impossible to fully align the beam. An aggressive effort was made to resolve the accelerator

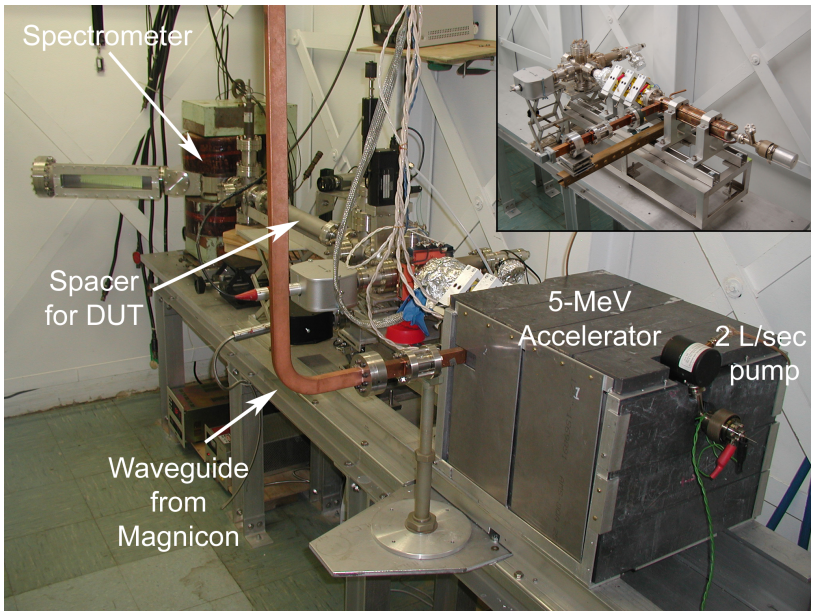


***Fig. 8.*** *Photograph of 5-Mev X-band accelerator beamline in bunker in the Magnicon Laboratory. Upper inset shows accelerator without lead shielding in place.*

problems, including replacement of the cathode assembly with a new $CeB_6$ cathode, followed by bakeout and reconditioning of the accelerator up to the operating power level.

Over time, however, a number of difficulties were encountered during day-to-day operation. The first can be described as transient cathode poisoning, where the emission current decreases over a number of pulses. This may be due to poor vacuum conditions near the cathode, perhaps caused by limited pumping conductance. In 2015 we reduced the rep rate from a few pulses per second to 0.25 Hz, and the stability and pressure improved. The second problem is intermittent arcing in the accelerator, likely in the first cell (near the cathode). Arcing occurs more frequently when the cathode is hot, and depends upon the exact position of the cathode in the first cell. A third problem was a vacuum leak on the feedthrough for the cathode heater leads. Measurements indicated that significant rf power was leaking past the cathode, and may have caused the vacuum leak. A new cathode assembly with an improved rf choke was inserted into the accelerator, which resulted in significantly less rf leakage.

In 2015, an rf probe was installed in the vacuum tube behind the cathode (near the 2 L/sec ion pump). This rf probe has proven to be a very useful diagnostic to observe operating conditions inside the accelerator. The dc component of the probe signal is rejected using a coax-to-waveguide transition, and a coax detector rectifies the signal that is then displayed on an oscilloscope. At relatively low rf power, the probe signal is smooth and is similar to the forward and reflected detector traces. As the rf power increases towards the breakdown regime, more complicated features often appear. On the leading edge of the pulse, the probe voltage begins to collapse, which indicates some instability in the cavity. It is also possible to observe collapse and high-frequency modulation during the peak and fall of the pulse. If the power is increased further and these features are allowed to grow, the reflected signal becomes distorted and a significant increase in pressure is observed on the 2 L/sec ion pump. The probe and reflected signals have been used to guide the conditioning process and improve stability during the last year.

The cathode stalk is mounted on a micrometer drive, which allows the cathode position to be adjusted while under vacuum. As the cathode is pushed further into the first cell, recent measurements show that the resonant frequency increases, the reflected power decreases, and the probe signal increases. Under these conditions, the accelerator is a better match at the magnicon frequency of 11.42 GHz. However, increased arcing is observed at high power when the cathode protrudes into the first cell, presumably due to large electric fields near the edge of the cathode. As the cathode is retracted, the

reflection coefficient increases somewhat and the probe signal decreases, but breakdown events are significantly reduced. Accelerator operation is much more stable with the cathode recessed, and forward powers up to 7 MW have been directed to the accelerator. There are two YAG screens (downstream from the accelerator) that are used to observe the electron beam during conditioning. Recent experiments have concentrated on increasing the energy of the electron beam while minimizing any arcing or disruptive behavior.

A number of experiments were performed during the last year to image the electron beam on the YAG screen while varying the experimental parameters, such as drive power, cathode heater current, cathode position, and beam focusing and steering. Two types of current are typically observed in the experiment: thermionic emission from the cathode and (possibly) electron emission from arcing. As the RF power is increased, the goal is to maximize the current from the cathode, and operate in a parameter space where arcing is minimized. We recently obtained separate images of the thermionic and arc-generated beams on the YAG screen. The surprising finding is that the two beams are not co-located, but offset in the horizontal direction. The separation between the two beams is relatively large, so that an aperture could be used to pass the main beam and block electrons that are generated by arcing. The fact that the two beams are not co-located is evidence that the arcing does not occur on the cathode surface. Research goals in the near future include varying the experimental parameters to minimize unwanted arcing and maximizing the current and energy of the thermionic beam.

5. The following recent papers and presentations acknowledged DoE support:


a. "Complete multipactor suppression in an X-Band dielectric-loaded accelerating structure," C. Jing, S.H. Gold, and R. Fischer, and W. Gai, *Appl. Phys. Lett.,* vol. 108, 193501 (2016).
b. "Experimental study of multipactor suppression in externally powered dielectric accelerating structures," C. Jing, R. Konecny, and S.H. Gold, presented at the Sixteenth Advanced Accelerator Concepts Workshop (AAC 2014), 13–18 June 2014, San Jose, CA and in the Proceedings of the Sixteenth Advanced Accelerator Concepts Workshop, in press.
c. "Study of multipactor loading in X-Band dielectric-loaded accelerating structures," S.H. Gold, C. Jing, W. Gai, A. Kanareykin, and A. Kinkead, presented at the Forty-First IEEE International Conference on Plasma Science, 25–29 May 2014, Washington, DC.
d. "Active microwave pulse compressor using an electron-beam triggered switch," O.A. Ivanov, M.A. Lobaev, A.L. Vikharev, A.M. Gorbachev, V.A. Isaev, J.L. Hirshfield, S.H. Gold and A.K. Kinkead, *Phys. Rev. Lett.,* vol. 110, 115002 (2013).
e. "Observation of multipactor suppression in a dielectric-loaded accelerating structure using a solenoidal magnetic field," C. Jing, C. Chang, S. H. Gold, R. Konecny, S. Antipov, P. Schoessow, A. Kanareykin, and W. Gai, *Appl. Phys. Lett*., vol. 103, 213503 (2013).
f. "Experiment on multipactor suppression in dielectric-loaded accelerating structures with a solenoid field," C. Jing, R. Konecny, A. Kanareykin, S. Antipov, P. Schoessow, C. Chang, L. Xiao, L. Ge, M. Conde, J.G. Power, W. Gai, and S. Gold, in the Proceedings of IPAC 2013, The 4th International Particle Accelerator Conference, 12–17 May 2013, Shanghai, China, paper TUPEA087.
g. "Active pulse compression results," A.L. Vikharev, O.A. Ivanov, M.A. Lobaev, A.M. Gorbachev, V.A. Isaev, J.L. Hirshfield, S.H. Gold, and A.K. Kinkead, presented at HG2013: International Workshop on Breakdown Science and High Gradient Technology, 3–6 June 2013, Trieste, Italy.
h. "Effect of an axial magnetic field on multipactor in a dielectric-loaded accelerating structure," S.H. Gold, C. Jing, W. Gai, A. Kanareykin, and A. Kinkead, presented at the IEEE Pulsed Power & Plasma Science Conference — PPPS 2013, 16–21 June 2013, San Francisco, CA.
i. "Test of a standing-wave dielectric loaded accelerating structure," C. Jing, S.P. Antipov, A. Kanareykin, P. Schoessow, W. Gai, and S.H. Gold, presented at the 2013 North American Particle Accelerator Conference, NA-PAC 2013, 29 September – 4 October 2013, Pasadena, CA.

j. “An X-band standing wave dielectric loaded accelerating structure,” C. Jing, S. Antipov, P. Schoessow, and A. Kanareykin, R. Konecny, S. Kazakov, and S. Gold, in the Proceedings of the 2012 International Particle Accelerator Conference, 20–25 May 2012, New Orleans, LA, pp. 1927–1929.
k. “High power X-band pulse compressor using electron beam switching,” Anatoly L. Vikharev, Aleksey M. Gorbachev, Oleg A. Ivanov, Mikhail Lobaev, Steven H. Gold, Jay L. Hirshfield, and Allen K. Kinkead, presented at the Fifteenth Advanced Accelerator Concepts Workshop—AAC 2012, 10–15 June 2012, Austin, TX.
l. “Test of an X-band standing wave dielectric accelerating structure,” C. Jing, S. Antipov, P. Schoessow, A. Kanareykin, J. Power, M. Conde, W. Liu, R. Konecny, W. Gai, S.H. Gold, C. Chang, V. Dolgashev, and S. Tantawi, presented at the Fifteenth Advanced Accelerator Concepts Workshop—AAC 2012, 10–15 June 2012, Austin, TX.
m. “Active X-Band pulse compressor using electron-beam switching,” S.H. Gold, A.L. Vikharev, A.M. Gorbachev, O.A. Ivanov, M. Lobaev, and A.K. Kinkead, presented at the Thirty-Ninth IEEE International Conference on Plasma Science, 8–12 July 2012, Edinburgh, UK.
n. “High gradient research at the Naval Research Laboratory,” Steven H. Gold, seminar presented at Purdue University, West Lafayette, IN, 21 September 2011.

6. The following individuals were supported during the last three years of this program (1 April 2013 – 31 March 2016):

Dr. Richard P. Fischer, PI
Dr. Steven H. Gold

Dr. Steven H. Gold, the initial PI of the program, retired from NRL on 2 January 2015. The new PI of the program is Dr. Richard Fischer of the NRL Plasma Physics Division. This change of PI was proposed on 28 October 2014 by Dr. Thomas A. Mehlhorn, Superintendent of the NRL Plasma Physics Division, and approved by Dr. Eric Colby of the DoE Office of High Energy Physics. Effective 5 January 2015, Dr. Gold became a paid contractor to NRL and continued to work on this research program.

7. Unexpended funds: None.